ACADEMIC PRESS

Available online at www.sciencedirect.com
SCIENCE DIRECT®

Journal of Solid State Chemistry 171 (2003) 439–443

JOURNAL OF SOLID STATE CHEMISTRY

http://elsevier.com/locate/jssc

$(ZrO_2)_{0.85}(REO_{1.5})_{0.15}$ (RE = Sc, Y) solid solutions prepared via three Pechini-type gel routes: 2—sintering and electrical properties

Yawen Zhang, Ang Li, Zhengguang Yan, Gang Xu, Chunsheng Liao, and Chunhua Yan*

State Key Lab of Rare Earth Materials Chemistry and Applications & PKU-HKU Joint Lab on Rare Earth Materials and Bioinorganic Chemistry, College of Chemistry and Molecular Engineering, Peking University, Beijing 100871, China

Received 25 April 2002; received in revised form 8 September 2002; accepted 12 September 2002

Abstract

Dense $(ZrO_2)_{0.85}(REO_{1.5})_{0.15}$ (RE = Sc, Y) specimens have been obtained from the nanoparticulate powders prepared by three Pechini-type gel routes, viz. poly(vinyl alcohol) (PVA) containing-process (route I), poly(ethylene glycol) and formic acid-containing process (route II), and in situ polymerizable complex method (route III). During sintering over 1000–1400°C, $(ZrO_2)_{0.85}(ScO_{1.5})_{0.15}$ samples prepared by routes II and III, and $(ZrO_2)_{0.85}(YO_{1.5})_{0.15}$ samples prepared by the three routes retain pure cubic fluorite structure, however, a monoclinic phase segregation takes place for the Sc-doped zirconia prepared by route I. Various gel routes are shown to display significant impact on sinterability of the green body, crystallinity and particle size uniformity of the sintered body, and the ionic conductivity of the dense specimens. The specimens prepared from route III exhibit superior sinterability and ionic conductance to those prepared from routes I and II.

Keywords: Sc- or Y-doped zirconia; Gel syntheses; Sintering process; Electrical properties

1. Introduction

For application in solid oxide fuel cells (SOFCs), ceramic electrolytes with good sinterability, improved electrical properties and long-term stability are required [1,2]. Besides calcination, the sintering process plays a very significant role in constructing the ceramic microstructures and hence governing the performance of the material.

During sintering/densification, crystallite coarsening, volume reduction, decrease in porosity and increase in grain size will occur for a green compact. Previously, Torrens et al. explored the effects of the synthesis routes including solid-state reaction and co-precipitation on the sinterability and electrical properties of $(CeO_2)_{0.8}(GdO_{1.5})_{0.2}$ polycrystalline specimens, and found that the powders synthesized via solid-state reaction showed much inferior results, even after sintering at 1650°C [3]. Up to now, similar researches, particularly concerning the influence of various gel routes on the sintering behaviors and ionic conductance of the ceramic electrolytes used in SOFCs, are still inadequate.

As promising electrolytes for SOFCs, $(ZrO_2)_{0.85}(REO_{1.5})_{0.15}$ (RE = Sc, Y) solid solutions requires a comprehensive knowledge of the relationship between the microstructures created by various synthesis routes and the associated properties [1]. Our previous paper [4] described the synthesis of $(ZrO_2)_{0.85}(REO_{1.5})_{0.15}$ (RE = Sc, Y) nanoparticles in pure cubic fluorite structure by three Pechini-type gel routes, viz. poly(vinyl alcohol) (PVA) containing-process (route I), poly(ethylene glycol) (PEG) and formic acid-containing process (route II), and in situ polymerizable complex method (route III). It was confirmed that the altered variety of polymer and cross-linking within the gels adopted by the three routes make the as-synthesized samples show appreciable differences in thermal behavior, powder reactivity and particle properties.

In this paper, we discuss how the three gel routes affect the sintering behavior and electrical properties of the specimens prepared from the as-obtained nanoparticles [4].

*Corresponding author. Fax: +86-10-6275-4179.
E-mail address: chyan@chem.pku.edu.cn (C. Yan).

0022-4596/03/$ - see front matter © 2003 Elsevier Science (USA). All rights reserved.
doi:10.1016/S0022-4596(02)00228-1

2. Experimental

2.1. Compacting and sintering

The gels prepared by the three Pechini-type gel routes were calcined at 800°C for 10 h to obtain nanoparticulate oxide powders. To prepare dense specimens, 0.15–0.4 g of the powders were ground for 15 min using an agate pestle and mortar, then uniaxially pressed into pellet specimens with a diameter of 6 mm under 12 MPa pressure. Finally, the specimens were sintered under static air at various temperatures (1000–1400°C) for 24 h.

The nomenclature and the preparative conditions of the samples are given in Ref. [4].

2.2. Characterization methods

The crystal structures were identified by a Rigaku D/max-2000 powder X-ray diffractometer, using Cu$K\alpha$ radiation ($\lambda = 1.5408$ Å). The percentage of the monoclinic phase was calculated from the relative peak area of the monoclinic (m) peaks $(11\bar{1})_m + (111)_m$ and the monoclinic plus cubic (c) peaks $(11\bar{1})_m + (111)_m + (111)_c$. The lattice parameters were calculated with least-squares methods. Considering that rare-earth cations occupy the Zr^{4+} sites to form a solid solution of $Zr_{1-x}RE_xO_{2-x/2}$, the theoretical density d_{th} can be calculated according to the following equation:

$$d_{th} = 4[(1-x)M_{Zr} + xM_{RE} + (2-x/2)M_O]/a^3N_A,$$

where $x = 0.15$; a, M and N_A are the calculated lattice parameter, atomic weight and Avogadro constant, respectively. In the case of the low-density specimens, the sintered density d_{exp} could not be measured by the water immersion technique owing to the fact that water can enter the pores in the sintered body [5]. For those specimens, the sintered density was estimated from the mass and geometric dimensions of the pellets. The relative density of the sintered body is given by d_{exp}/d_{th}. Samples with carefully polished surface were annealed for 30 min at 1000°C, and then, in selected cases, were platinum coated by ion sputtering. The microstructures were observed by scanning electron microscopy (SEM, KYKY-2800, China).

2.3. Electrical property measurements

The electrical properties of the dense specimens were determined in air by AC two-probe measurements on a frequency response analyzer (HP-4192A LF, 200 Hz–12 MHz) [6]. The impedance data points were collected with temperature intervals of 40°C on cooling over 800–400°C. Two Pt lead wire electrodes were adhered to two terminals of the specimen with Pt paste, which was fired at 800°C for 30 min to remove the polymeric components. The ionic conductivity was calculated from the intercepts of the observed semicircle on the real axis of the Cole–Cole plot with the "EQUIVCRT" software [7].

3. Results and discussion

3.1. Sintering behaviors

Upon sintering, a powder compact acquires densification under the driving force arising from the excess free energy associated with the surface area/particle size of the powder via pore removal and/or crystallite coarsening [8,9]. Good sinterability is represented by the compacts showing high sintered density, good particle size uniformity and good crystallinity after sintering.

Fig. 1 shows the XRD patterns of the SZ1, SZ2 and SZ3 specimens. The SZ2 and SZ3 specimens maintain the pure cubic structure over 1000–1400°C. However, the SZ1 specimen shows a mixture of predominately cubic phase and a little monoclinic phase, meaning that the segregation of m-ZrO_2 occurred during sintering over 1000–1400°C, even if the pre-sintered powders were in pure cubic phase owing to the crystallite size effect [4]. The monoclinic phase fraction for the SZ1 sample increased from 4.1% at 1000°C to 6.7% at 1200°C and 18.7% at 1400°C. The appearance of m-ZrO_2 for the sintered SZ1 sample is possibly caused by the chemical inhomogeneity of the microdomains, correlative with the segregation of some metal ions into sol or colloid during the gel formation in route I. Yashima et al. also reported the formation of sol or colloid could lead to the compositional inhomogeneity and thus the phase

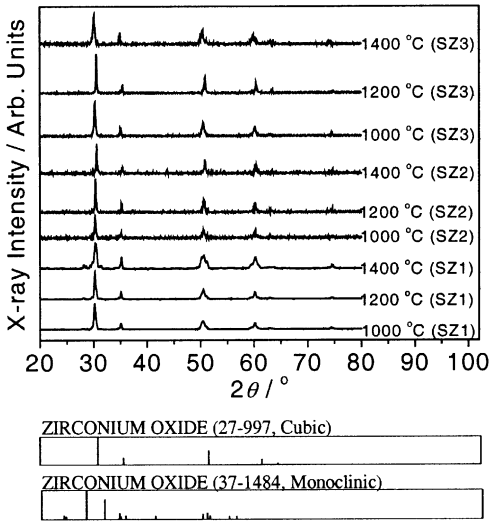

Fig. 1. XRD patterns of the SZ1, SZ2 and SZ3 specimens sintered over 1000–1400°C.

splitting in preparing $(ZrO_2)_{1-x}(CeO_2)_x$ ($x = 0.2,\ 0.5$) solid solutions [10].

The XRD patterns of YZ1, YZ2 and YZ3 showed these samples crystallized in pure cubic phase after sintering over 1000–1400°C. The difference in phase purity exhibited by YZ1 and SZ1 strongly suggest that doping of yttria into zirconia is much easier than that of scandia. On the other hand, it is concluded that strong coordination in the gels prepared by routes II and III can effectively prevent the metal ions from segregating and hence improve the chemical homogeneity of the precursors. The enhanced chemical homogeneity can make the samples avoid phase segregation upon sintering.

The values for the lattice parameter, a, of the as-prepared specimens were found to be independent of sintering temperatures and the synthesis route used in this study, but depend upon the variety of the dopants. The average values of a for $(ZrO_2)_{0.85}(REO_{0.15})_{0.15}$ (RE = Sc, Y) are about 5.10 and 5.14 Å, respectively, which are consistent with the data previously reported [11–13].

At 1000°C, 1200°C and 1400°C, the sintered densities of the six samples are in the range of 3.27–3.80, 4.01–4.46 and 4.12–5.16 g cm^{-3}, respectively. On the other hand, it was observed that, for all samples, the sintered density increases with sintering temperature, meaning that sintering at high temperature can assist the specimen of processing to acquire full densification.

Fig. 2 depicts the relative density of the six specimens as a function of sintering temperature. We clearly see that the sintered densities of SZ3, YZ3, YZ1 and SZ2 increase rapidly as the temperature is raised from 1000°C to 1400°C. In particular, it is noteworthy that the relative density of the SZ3 and YZ3 specimens sintered at 1400°C is up to 81% and 88%, respectively.

Typical SEM micrographs of Sc-doped zirconia samples sintered at 1000°C are displayed in Fig. 3. These micrographs show agglomerates in the three

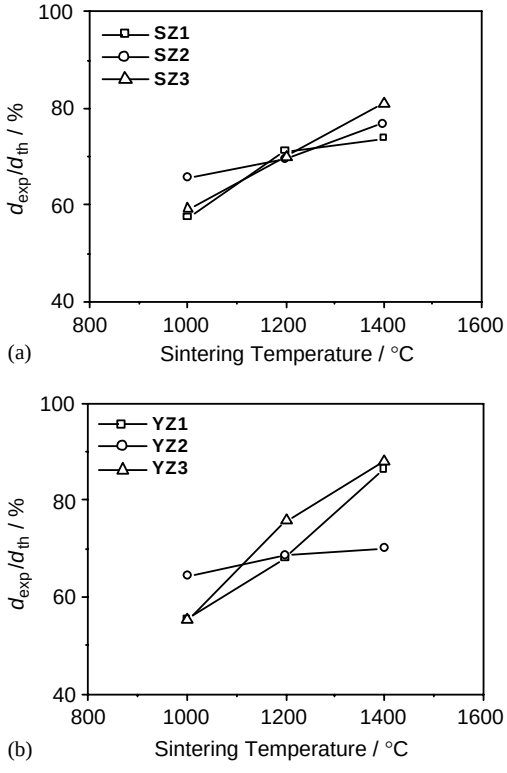

Fig. 2. Relative density of the SZ1, SZ2, SZ3, YZ1, YZ2 and YZ3 specimens as a function of sintering temperature.

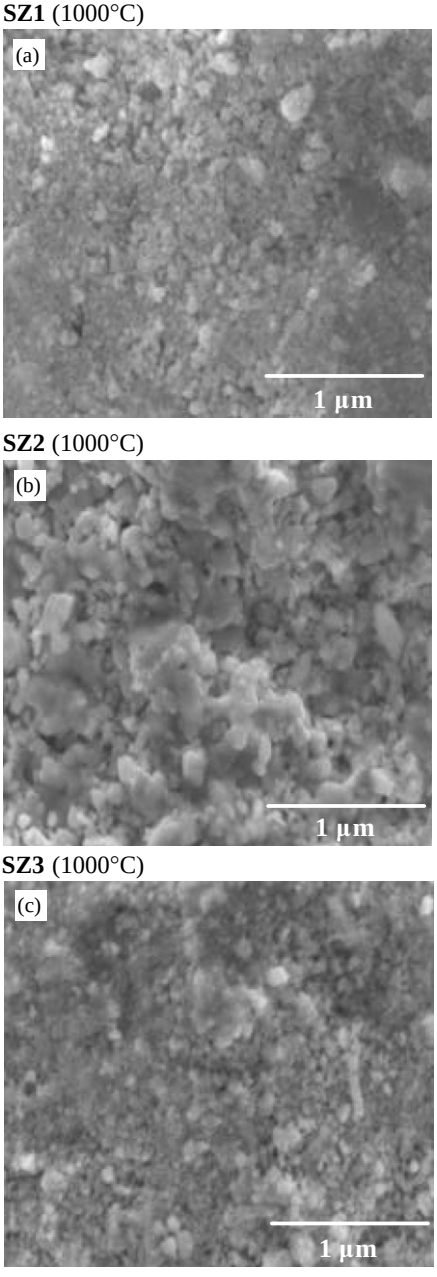

Fig. 3. SEM micrographs of the SZ1 (a), SZ2 (b) and SZ3 (c) specimens sintered at 1000°C.

samples, which are composed of irregular particles of hundreds of nanometers at this temperature. It is also noteworthy that the particles in the specimens derived from route III are more uniform. At 1000°C, the grain size of the three samples is estimated to be 150–200 nm. After sintering at 1200°C and 1400°C, respectively, the grains grow significantly and tend to be faceted with increasing the sintering temperature, indicating a gradual increase in crystallinity. Among the six samples, SZ3 and YZ3 derived from route III still exhibit better size uniformity, hinting that the gels prepared by route III are the most homogeneous. The enhanced homogeneity corresponds to the strongest coordination between metal ions and the rigid polymers throughout the gels prepared by this route, as proposed in the previous paper [4]. At 1200°C and 1400°C, the grain size of the six samples is in the range of 0.3–0.7 and 0.6–1.5 μm, respectively.

From the above discussions, it is concluded that the compacts derived from the nanoparticulate powders prepared by the in situ polymerizable complex method exhibit fairly good sinterability, due to the best chemical homogeneity of the gels [4].

3.2. Electrical properties

Fig. 4 is the Arrhenius plot of bulk ionic conductivity. For all the samples, the bulk conductivity σ_b increases with increasing the sintering temperature/density from 1000°C to 1400°C, as was also observed for $(ZrO_2)_{0.85}(REO_{1.5})_{0.15}$ (RE = Sc, Y) polycrystalline [13]. Low sintered densities not only decrease the bulk conductivity, but also the grain boundary conductivity [5,13]. In addition, Okubo et al. concluded that the presence of pores in sintered body could impair the conduction path between grains, and thus reduce the conductivity [14].

Over 480–640°C, $\sigma_b(SZ3) \gg \sigma_b(SZ2) \approx \sigma_b(SZ1) > \sigma_b(YZ3) \approx \sigma_b(YZ1) > \sigma_b(YZ2)$ [Fig. 4(a)], $\sigma_b(SZ3) \gg \sigma_b(SZ2) \approx \sigma_b(SZ1) > \sigma_b(YZ3) > \sigma_b(YZ1) > \sigma_b(YZ2)$ [Fig. 4(b)], and $\sigma_b(SZ3) \approx \sigma_b(SZ2) \gg \sigma_b(YZ3) \approx \sigma_b(YZ1) > \sigma_b(SZ1) > \sigma_b(YZ2)$ [Fig. 4(c)] are observable for the samples sintered at 1000°C, 1200°C and 1400°C, respectively. The SZ3 and YZ3 samples typically show the highest bulk conductivity among the same kind of electrolytes at a given temperature, perhaps owing to their good compositional homogeneity, uniform grain size distributions and well-defined crystallite shape, as previously observed. In most cases, for the samples prepared by the same route, σ_b for the Sc-doped zirconia sample is higher than that for the Y-doped zirconia sample at a given temperature. This is consistent with the order of ionic conductivity for the rare earth stabilized zirconia [11]. An exception occurs for the SZ1 and YZ1 samples sintered at 1400°C. Owing to the fact that SZ1 contains 18.7% of m-ZrO_2, which is non-ion-conductive, $\sigma_b(SZ1)$ is slightly smaller than $\sigma_b(YZ1)$. The conductivity activation energies E_a for the bulk process are summarized in Table 1.

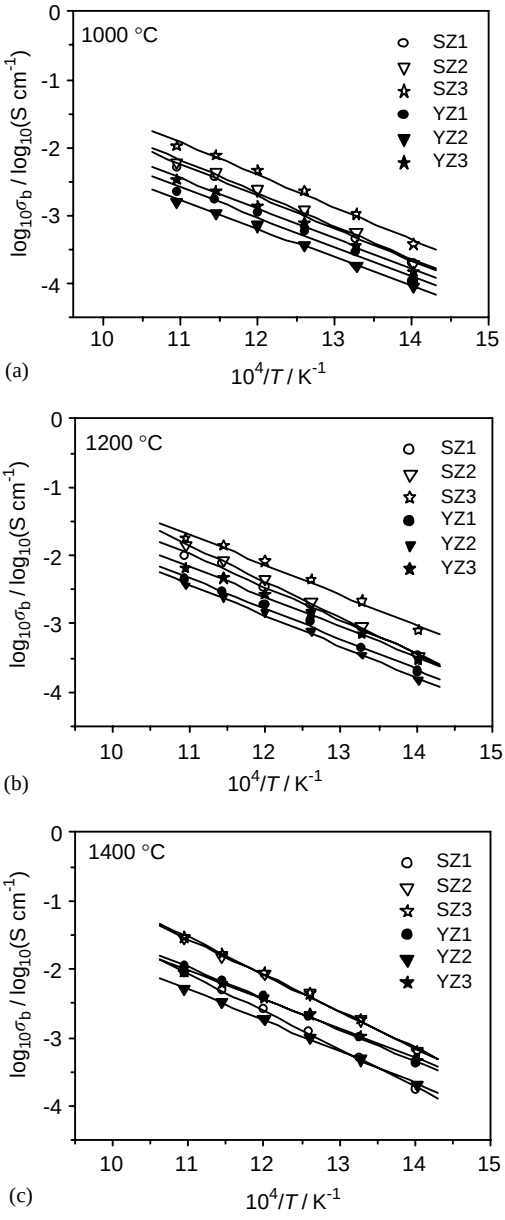

Fig. 4. Arrhenius plot of $\log_{10}\sigma_b$ vs. $1/T$ for the SZ1, SZ2, SZ3, YZ1, YZ2 and YZ3 specimens sintered at 1000°C (a), 1200°C (b) and 1400°C (c).

For all the samples, the grain boundary conductivity σ_{gb} increases with the sintering temperature/density from 1000°C to 1400°C. Over 440–640°C, $\sigma_{gb}(SZ3) > \sigma_{gb}(SZ1) > \sigma_{gb}(SZ2) > \sigma_{gb}(YZ3) \approx \sigma_{gb}(YZ1) \gg \sigma_{gb}(YZ2)$, $\sigma_{gb}(SZ3) > \sigma_{gb}(SZ1) \approx \sigma_{gb}(YZ3) \gg \sigma_{gb}(SZ2) > \sigma_{gb}(YZ1) \approx \sigma_{gb}(YZ2)$, and $\sigma_{gb}(SZ3) \approx \sigma_{gb}(SZ2) \approx \sigma_{gb}(YZ3) > \sigma_{gb}(YZ1) \gg \sigma_{gb}(YZ2) > \sigma_{gb}(SZ1)$ are noticed for the samples sintered at 1000°C, 1200°C and 1400°C, respectively. Just as is the case for the bulk conductivity, the SZ3 and YZ3 samples typically show

Table 1
Activation energies for bulk (*b*) and grain boundary (gb) conductivity of the samples at various sintering temperatures

Sample	E_a[a]					
	1000°C		1200°C		1400°C	
	b	gb	*b*	gb	*b*	gb
SZ1	91	123	93	121	106	130
SZ2	93	119	102	117	102	110
SZ3	91	120	86	120	104	110
YZ1	83	106	86	102	88	113
YZ2	80	105	88	107	87	105
YZ3	85	104	84	121	81	105

[a] Uncertainties are ± 5/kJ mol^{-1}.

the highest bulk conductivity among the same kind electrolytes at a given temperature, possibly due to their high sintered density, well-defined grain shape and homogeneous grain boundary structure created by their good sinterability as mentioned above. The conductivity activation energies E_a for the grain boundary process are also listed in Table 1.

Generally, σ_{gb} values are affected by many factors such as porosity of the sintered body and impurities segregating to the grain boundaries [5,15], thus, elimination of the pores and the impurities in a given specimen as much as possible can enhance its grain boundary conductivity. Hereby, it appears that the samples having high bulk conductivity and sintered density (with as few pores as possible) also show relatively high grain boundary conductivity.

4. Conclusion

Upon sintering over 1000–1400°C, $(ZrO_2)_{0.85}(ScO_{1.5})_{0.15}$ samples prepared by routes II and III, and $(ZrO_2)_{0.85}(YO_{1.5})_{0.15}$ samples prepared by the three routes maintain the ideal cubic fluorite structure, however, a monoclinic phase segregation takes place for the Sc-doped zirconia prepared by route I. It is shown that various synthesis gel routes used in this work display significant impact on the sinterability of the green body, the crystallinity and the particle size uniformity of the sintered body, and the ionic conductivity of the dense specimens. Both the bulk and grain boundary conductivities increase with increasing sintering temperature/density, and depend on not only the variety of dopants but also the synthesis route used. Among the as-prepared samples, those prepared by the in situ polymerizable complex method show the best sinterability, and exhibit the highest bulk and grain boundary conductivities, owing to the best chemical homogeneity on the molecular level in the gels achieved by this method. The enhanced chemical homogeneity was achieved by the existence of the strongest coordination between metal ions and the rigid polymer nets throughout the gels. It is concluded that the microstructures and electrical properties of ceramic electrolytes can be tailored by employing rational gel route and controlling the coordination between metal ions and polymers in the gels.

Acknowledgments

Grants-in-aid from MOST of China (G1998061300), NSFC (Nos. 20171003, 29832010 & 20023005) and Founder Foundation of Peking University are gratefully acknowledged.

References

[1] J. Drennan, J. Mater. Synth. Process. 6 (1998) 181.
[2] S.P.S. Badwal, Solid State Ionics 143 (2001) 39.
[3] R.S. Torrens, N.M. Sammes, G.A. Tompsett, Solid State Ionics 111 (1998) 9.
[4] Y.W. Zhang, A. Li, Z.G. Yan, G. Xu, C.S. Liao, C.H. Yan, J. Solid State Chem. (2002) (RERC paper PSS-47)
[5] I.R. Gibson, G.P. Dransfield, J.T.S. Irvine, J. Mater. Sci. 33 (1998) 4297.
[6] J.E. Bauerle, J. Phys. Chem. Solids 30 (1969) 2657.
[7] B.A. Boukamp, EQUIVCRT Software, University of Twente, Enschede, The Netherlands.
[8] F.F. Lange, J. Am. Ceram. Soc. 72 (1989) 3.
[9] J.G. Li, T. Ikegami, T. Mori, T. Wada, Chem. Mater. 13 (2001) 2921.
[10] M. Yahima, K. Ohtake, M. Kakihana, M. Yoshimura, J. Am. Ceram. Soc. 77 (1994) 2773.
[11] D.W. Strickler, W.G. Carlson, J. Am. Ceram. Soc. 48 (1965) 286.
[12] H.G. Scott, J. Mater. Sci. 10 (1975) 1527.
[13] Y.W. Zhang, Y. Yang, S. Jin, C.S. Liao, C.H. Yan, J. Mater. Chem. 11 (2001) 2067.
[14] T. Okubo, H. Nagamoto, J. Mater. Sci. 30 (1995) 749.
[15] M. Aoki, Y.-M. Chiang, I. Kosacki, L.J.–R. Lee, H.L. Tuller, Y.P. Liu, J. Am. Ceram. Soc. 79 (1996) 1169.